Final Draft
of the original manuscript:

Maier, P.; Lauth, N.; Mendis, C.L.; Bechly, M.; Hort, N.:
Mechanical and Corrosion Properties of Two Precipitation-Hardened Mg-Y-Nd-Gd-Dy Alloys with Small Changes in Chemical Composition.
In: JOM: Journal of the Minerals, Metals and Materials Society. Vol. 71 (2019) 4, 1426 - 1435.
First published online by Springer: February 06, 2019

DOI: /10.1007/s11837-019-03359-1
https://dx.doi.org/10.1007/s11837-019-03359-1

Mechanical and Corrosion Properties of Two Precipitation-Hardened Mg-Y-Nd-Gd-Dy Alloys with Small Changes in Chemical Composition

P. Maier[1] and N. Lauth[1], C. L. Mendis[2], M. Bechly[1], N. Hort[3]

[1]University of Applied Science Stralsund, Stralsund, Germany
[2]Brunel University London, Brunel Centre for Advanced Solidification Technology, London, UK
[3]Magnesium Innovation Centre, Helmholtz-Zentrum Geesthacht, Max-Planck-Strasse 1, 21502, Geesthacht, Germany

Abstract

Precipitation hardening in Mg-Y-Nd alloys (WE-type) is based on finely dispersed particles offering an effective strengthening mechanism to achieve high strength at moderate ductility. However, these particles often affect corrosion by being more noble than the matrix. Biodegradable implant materials should show a corrosion rate fit to its application but should be free of pitting corrosion. Especially deep and narrow pits act as notches and cause increased mechanical stress leading into early failure. WE43 has already shown to have an acceptable biological response. In this study, two Mg-Y-Nd-Gd-Dy alloys, WE32 and WE33, in extruded, solution and precipitation heat-treated conditions have been investigated. The difference in alloy composition is not very high. Solution heat treatment (T4) causes grain growth and strength loss. The ageing response to peak hardness depends on the temperature. A rather short ageing response was observed for 250°C, and highest hardness has been found for 200°C at longer ageing time but higher hardness compared to 250°C. Grain growth during ageing is not significant. The higher alloyed alloy WE33 shows better mechanical strength, but less ductility. Corrosion was evaluated with immersion and potentiodynamic polarization in Ringer Acetate solution. The corrosion rate strongly depends on the alloy and heat-treatment condition as well as on the test method. The highest corrosion rate is observed in the solution-treated condition. The peak aged alloy shows the lowest corrosion rate, but non-uniform corrosion and has been evaluated by the pitting factor.

1 Introduction and Motivation

The commercial alloy WE43 (Mg-4Y-3RE, where RE is mostly a mixture of rare-earth elements like Ce or Nd) is preferentially under investigation as implant materials. WE43 is an alloy with an acceptable biological response, relatively slow degradation in aqueous solutions, good electrochemical properties and excellent mechanical and corrosion properties [1,2]. Therefore, WE43 alloy is suggested to be a suitable candidate for implant application material [3-5] and is already applied as bone screws and stents [6,7]. Two hot-extruded Mg-Y-RE alloys are used in this study and contain slightly smaller amounts of total alloying additions compared with the commercial WE43 [8] Alloys of WE-type are conventionally used in the precipitation-hardened (T6) condition and the intermetallic particles are fully characterized [9-12]. Intermetallic particles, $Mg_{12}Nd$ and $Mg_{14}Y_4Nd$, are both observed in Mg-Y-Nd and the mechanical properties of the alloy depend strongly on the volume fraction and spatial distribution of these intermetallic phases.

This work investigates the influence of the intermetallic particles of two extruded alloys, containing small amounts of Gd and Dy in addition to Y and Nd, on their mechanical properties, mostly by looking at the hardness and corrosion properties, and especially the corrosion rate and corrosion morphology. Two Mg-Y-Nd-Gd-Dy alloys with small changes in chemical composition have been studied. Gd in Mg forms Mg_5Gd, which acts as beneficial on corrosion behavior while its acute toxicity is only moderate [13]. Mg-Dy alloys show a uniform corrosion behavior and good cytocompatibility [14]. In biomedical applications, an appropriately slow (to avoid fast hydrogen evolution), uniform corrosion is needed. Corrosion pits cause under additional mechanical loading increase stress intensity and act as crack tips, which should be avoided. Where pitting is the predominant form of attack, the extent and type of pitting may be evaluated in accordance with ASTM G46-76 [15] Deep and narrow pits as well as undercutting pits are most harmful; wide and shallow pits are least harmful.

The pitting factor is calculated by p/d, where p is the deepest penetration and d the average penetration depth. Either cross-sectional micrographs or 3D light microscopy imaging evaluates the value p [16,17]. The average penetration depth d is either evaluated by the corrosion rate by the weight loss method for the immersion tests or by the average depth of the corroded area of the cross-sectional micrograph. However, pits may overlap to give the appearance of a rough surface. High pitting factor values indicate a greater susceptibility to pitting corrosion, while a pitting factor of 1 relates to a uniform corrosion. A study by Witte [18] presents pitting factors up to 4.3 for the in vivo corrosion of LAE442 after 12 weeks. The mechanical properties required for bone implants are still under discussion; they should maintain mechanical integrity over a time scale of 12-18

weeks while the bone tissue heals and is replaced by natural tissue. The allowable strength loss depends on the application itself and is influenced by the bone density and extent of damage on the bone fracture.

2 Experimental

Alloys investigated were cast at Helmholtz-Zentrum Geesthacht under a protective gas mixture of Ar and 2% SF_6 and then hot-extruded at the Extrusion Research and Development Center TU Berlin at an overall temperature of 420°C, a product speed of 2.2 m/min and an extrusion ratio of 37. For the analysis of the overall chemical composition, inductively coupled plasma-optical emission spectroscopy was applied.

The alloys were solution-treated (T4) at 525°C for 8 h and quenched in warm water at 55°C to avoid quenching stresses. Precipitation hardening (T6) was carried out at 200°C and 250°C. Lower ageing temperatures will lead to higher peak age hardness,11 but a higher ageing temperature keeps the time for peak ageing low and the ductility at a moderate level. In accordance with,12 peak ageing at 250°C was expected within 10 h. To avoid natural ageing, the T6 treatment was carried out within a few hours after T4 or samples were stored at refrigerator temperatures. The samples (discs with a diameter of 17 mm) for metallographic and hard-ness investigations were prepared according to Kree [19]. The line inspection method was used for grain size measurements. To evaluate the influence of the heat treatment on corrosion, smaller cylin-ders (overall diameter of 14 mm and height of 10 mm) were used in potentiodynamic polarization under application of Ringer-Acetate solution (consisting of 1 L solution of 6 g sodium chloride, 3.7 g sodium acetate, 0.134 g calcium chloride, 0.203 g magnesium chloride and 0.4 g potassium chloride), with an initial pH value of 6.5. The solution was applied at a constant temperature of 37°C to fit body temperature. The potentiodynamic measurements were conducted on samples immediately after grinding with 1200-mesh paper and cleaning in an ultrasonic bath in ethanol. A three-electrode flow cell using a counter electrode, an Argenthal refer-ence electrode and a working electrode (with a measurement area of $\sim$ 95 mm^2; diameter of 11 mm) was used to evaluate polarization (current density-potential) curves (glass chamber cell volume $\sim$ 170 mL).

A flow rate of 8 L/min (overall electrolyte volume was 3.6 L) was used to keep the pH value below 8.5. Li et al. [20] have shown that the local corrosion behavior and the corrosion rate are strongly dependent on the flow of the electrolyte and that WE43 is more susceptibletocorrosioninaflowingsolution.Theshear stress applied by the flow promotes local corrosion, while static tests usually show lower corrosion rates. To force the Mg alloy into strong anodic corrosion, the curve

was traced with a scan rate of 50 mV/min from the negative potential end of $\sim$ 2000 mV towards the positive end of + 500 mV. The key point of this measurement is to study the passive/transpassive behavior and corrosion morphology. The passive/transpassive behavior is described by passivation current density and potential as well as the passive or pseudo-passive current density. Within the passive zone, the current density decreases significantly with increased potential (within the anodic corrosion part of the curve), where the pseudo-passive zone shows static current density values.

Furthermore, immersion tests were performed using three samples for each condition. The cylindrical samples had a diameter of 15 mm and a height of 10 mm and were exposed to 500 mL at 37°C for 7 days. The solution was changed after 4 days to avoid an increase in pH value above 8.5. The weight loss was measured by removing the corrosion products with chromic acid. The mean corrosion rate was measured by using the following equation, where Dm is the weight change in g, A the surface area sample in cm^2, t the immersion time in h and q the density in g/cm^33:

$$CR_m = \frac{8.76 * 10^4 * \Delta m}{A * t * \rho} \tag{1}$$

Corrosion behavior was discussed by considering the visual changes of the sample surface using light microscopy and the corrosion morphology was evaluated via 3D imaging and measurements on the cross-sectional micrographs after sectioning. For determination of the pitting factor, the deepest pit depth p is divided by the average penetration depth d. To evaluate p, either cross-sectional micrographs or 3D light microscopy imaging is used. The average penetration depth d of the immersion test is evaluated by the corrosion rate using the weight loss method and calculated for 7 days of exposure. In polarization, d is calculated by the corroded area of the cross-sectional micrograph and divided by the diameter of exposed area, here $\sim$ 11 mm.

Tensile properties were measured at room temperature with a TIRA mechanical testing machine at an initial speed of 2.4 mm/min. Cylindrical samples, at least 5 per condition, with a gauge length of 20 mm and a diameter of 6 mm, were used according to DIN EN ISO 6892-1. Vickers hardness (HV1) was tested with a universal hardness-testing machine ZHU2.5 using a Zwick hardness tester. The sample surface was ground after cutting to reduce residual stresses, and approximately 30 indents per test condition under a load of 1 kg (9.807 N) were carried out and the averages are reported.

3 Results and Discussion

Both the alloys used were named on the basis of WE43: WE32 for Mg2.78Y1.43Nd 0.43Gd0.41Dy and WE33 for the higher-alloyed alloy Mg3.05Y-1.81Nd0.50Gd 0.43Dy. In the hot extruded condition, WE32 has a hardness of 67.2 $\pm$ 2.1 HV1 and WE33 of 66.4 $\pm$ 4.5 HV1. The grain size of WE32 is at 15 $\pm$ 7.9 μm smaller than of WE33 at 21 $\pm$ 5.8 μm. There is no significant difference in hardness. Therefore, the similar measured hardness values are due to a counterbalance between the effect of grain size and alloying element concentration.

Figure 1a and b shows the hardness and grain size profiles of WE32 and WE33 influenced by the heat treatment; the supersaturated α-phase (T4) shows lower hardness, and ageing (T6) shows a hardening response. The hardness decrease during T4 is explained by the increase in grain size and the dissolution of the majority of the intermetallic particles. The grain growth in WE33 is more pronounced (140 μm in WE33 compared to 102 μm in WE32). Undissolved second phases could hinder the grain boundary mobility. The two alloys have different textures: WE33 has a pronounced non-basal texture with an intensity up to 6.5 for identification (10-10), whereas WE32 has a lower basal texture with an intensity up to 2.1 for (0001). How the higher amount of alloying additions influences the texture of this alloy is still under investigation, but an influence on preferred grain growth cannot be ruled out. The peak hardness during precipitation hardening strongly depends on the ageing temperature. Ageing at 250°C already leads to the peak aged condition after 8 h, with WE33 reaching a slight hardness of 79.8 HV1 compared to 77.3 HV1 of WE32 (Fig. 1a). The higher amount of alloying additions will increase the volume fraction of precipitates forming during T6. The grain size does not change much: a slight increase can be seen for WE33, whereas WE32 decreases slightly. In a study on another WE33 alloy, in which precipitation hardening on a Mg-3.3Y-3.4Nd alloy was investigated [21] a strong decrease in grain size during ageing was found. It is shown that a reduction in the mean value of grain size is likely to be based on the development on new fine grains during precipita-tion hardening, when recrystallization seems not to be finished during solution heat-treatment. Ageing at 200°C leads to a higher hardness but takes longer times: 92.7 HV1 of WE33 and 91.4 HV1 of WE32 (Fig. 1b).

Figure 2 shows the microstructural changes during thermomechanical processing and the condi-tions as-extruded (Fig. 2a and b), T4 solution heat-treated (Fig. 2c and d), T6 precipitation hardened at 250°C for 8 h (Fig. 2e and f) and precipitation-hardened at 200°C for 48 h (Fig. 2g and h). The remaining black spots in the micrographs indicate that, after solution heat-treatment, not all the intermetallic phases are dissolved. Apart from Nd, where the maximum solubility of 3.6 wt.% at the eutectic temperature of 545°C [22,23] decreases drastically with decreased temperature, the other alloying elements are below their maxi-

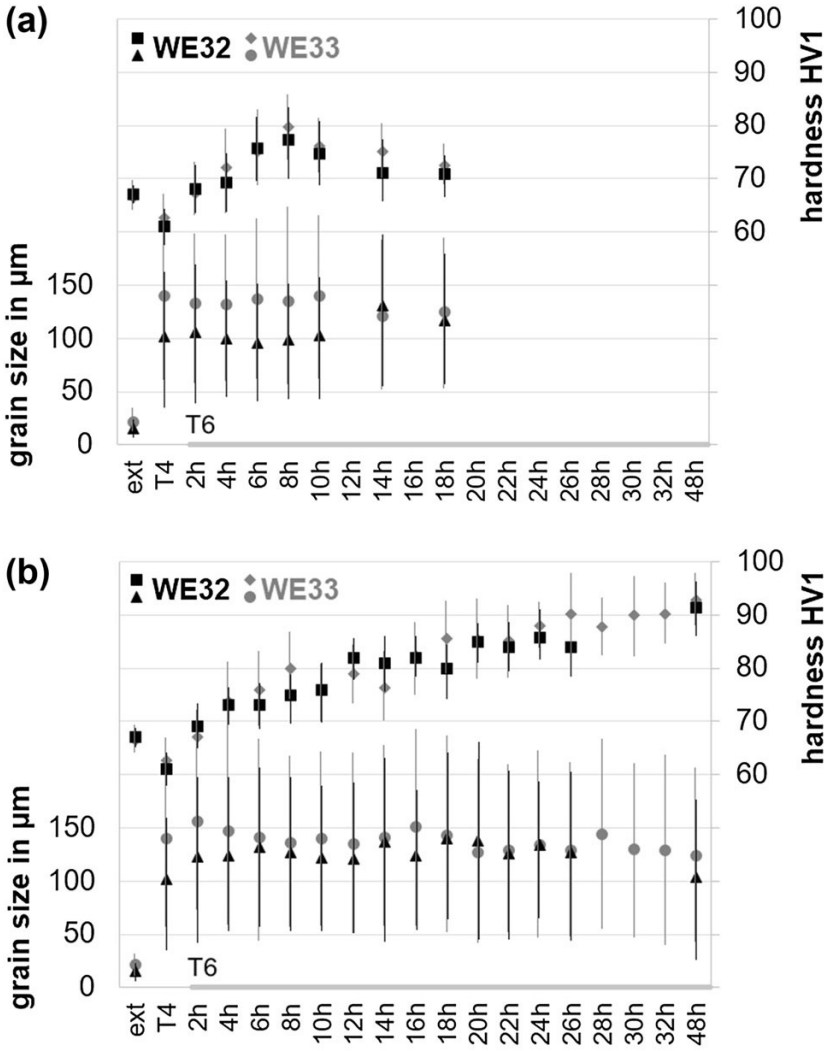

Figure 1: Influence of T4 and T6 heat-treatment on hardness and grain size of extruded WE32 and WE33 in dependence of ageing temperature: (a) 250°C and (b) 200°C.

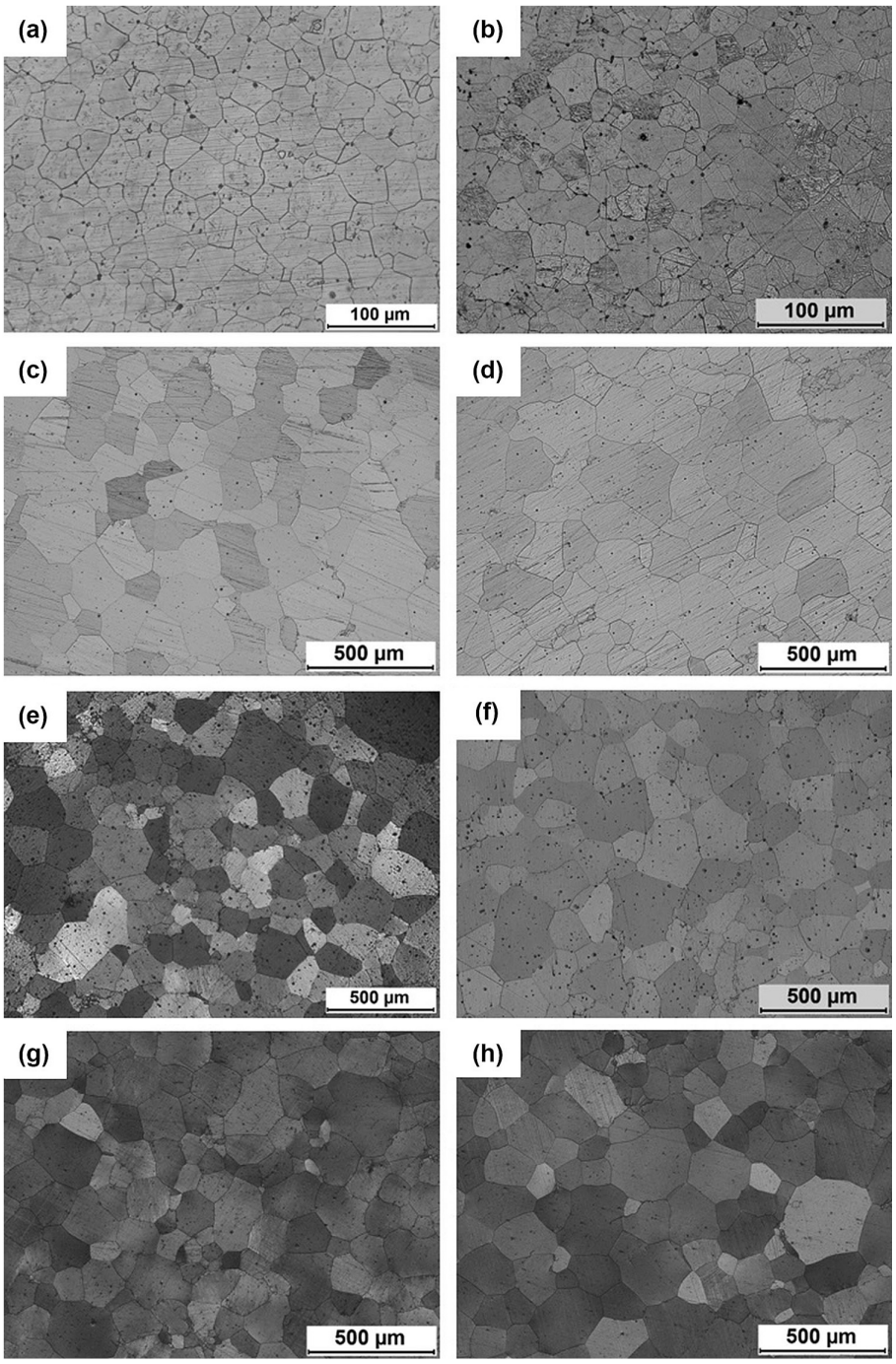

Figure 2: Microstructure of extruded WE32 (a, c, e, g) and WE33 (b, d, f, h): (a, b) extruded, (c, d) T4, (e, f) T6-250°C-8 h and (g, h) T6-200°C-48 h. Mechanical and Corrosion Properties of Two Precipitation-Hardened Mg-Y-Nd-Gd-Dy Alloys with Small Changes in Chemical Composition 1429

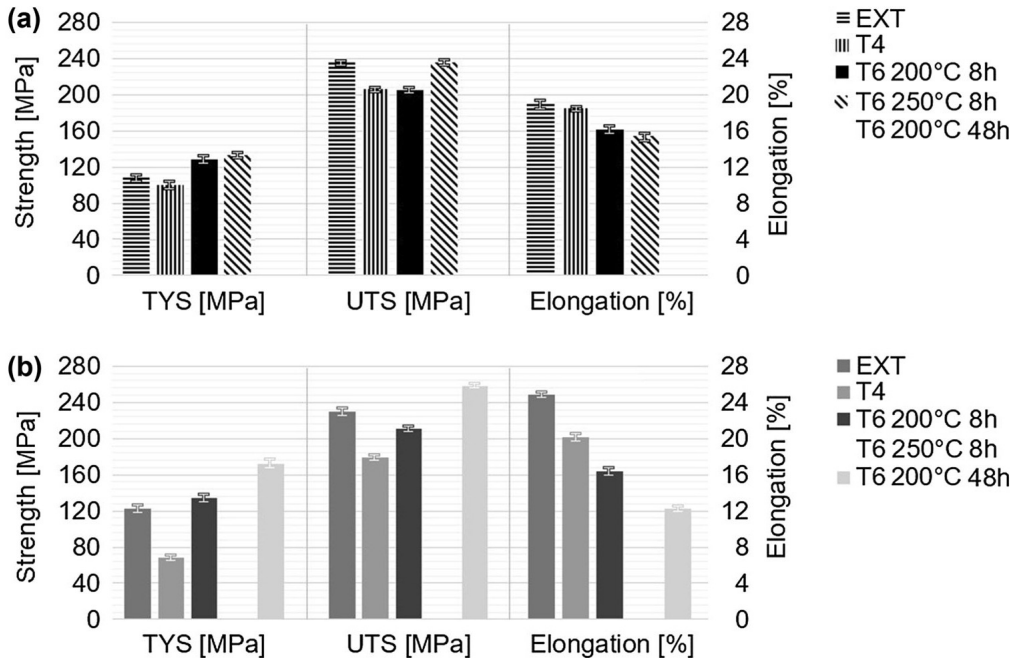

Figure 3: Influence of heat treatment T4 and T6 on tensile properties of extruded WE32 (a) and WE33 (b); there are no data for WE32-T6-200°C-48 h and WE33-T6-250°C-8 h.

mum solubility according their binary phase diagrams. WE33 (Fig. 2d) shows, a coarser average grain size compared to WE32 (Fig. 2c), in agreement to Fig. 1a and b. Precipitation hardening darkens the optical microscopy images in general (Fig. 2e-h), indicating the formation of precipitates. There are no significant visible changes of the microstructure during ageing, apart from the visibility of larger precipitates indicated by the black spots after ageing at 250°C for 8 h (see Fig. 2e and f). These spots are less significant after ageing at 200°C for 48 h, indicating that the precipitates causing the higher hardness of these conditions are much smaller.

In addition to the hardness measurements, tensile tests have been conducted. Figure 3 shows the influence of the heat treatment on strength and ductility. In WE33-T6-200°C-8 h, in agreement with the higher hardness, a slightly higher tensile yield strength (TYS) was observed. The higher ductility of WE33 can be explained by the higher amount of alloying additions, which may increase the activation of the basal slip due to the more random nature of the texture in WE33.

Solution heat treatment (T4) reduces TYS and ultimate tensile strength because of the dissolution of most intermetallic particles and reduces ductility due to the increased grain size. Unexpectedly, the decrease in strength is higher in

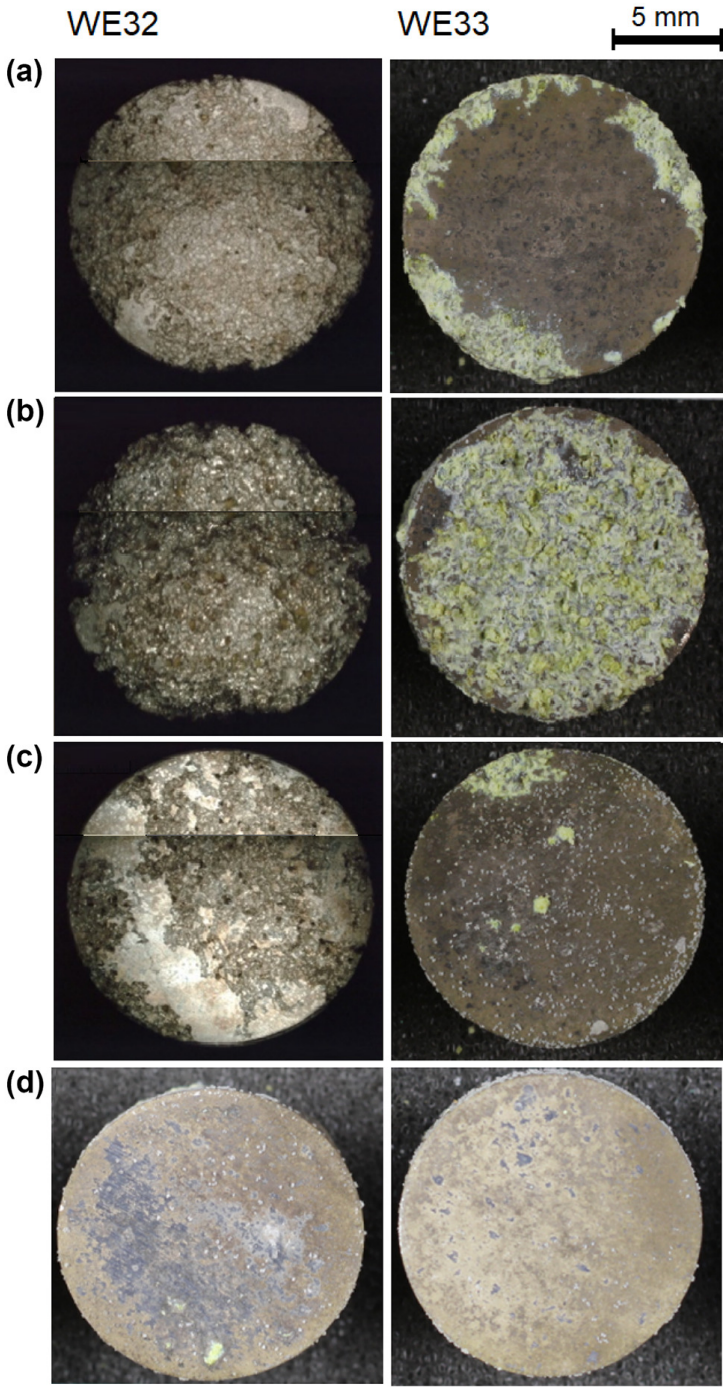

Figure 4: Top views of corroded samples of WE32 (left) and WE33 (right) in immersion over 7 days: (a) extruded, (b) T4, (c) T6-250°C-8 h and (d) T6-200°C-48 h.

WE33. In agreement with the hardness, TYS values exceed the initial strength when precipitation hardening (T6) was carried out over 8 h in WE32, while ageing at 250°C over 8 h shows a higher strength than at 200°C. There are no tensile properties of WE32-T6-200°C-48 h and WE33-T6-250°C-8 h due to lack of material. The elongation reduces after precipitation hardening. Previous research [24] on WE32 has shown a cup and cone fracture for the extruded condition with typical features of a ductile fracture and a more complex failure mode for the heat-treated conditions: a mix of ductile features like dimples accompanied by cleavage fracture parts in rather larger grains has been found. WE33 shows a slightly higher ageing response, especially at 200°C for longer ageing times (48 h). However, the strength increase is at the expense of the ductility. The smallest value among this series with 12.2% has been determined. Apart from the T6-200°C-48 h condition of WE33, the ultimate tensile strength values do not exceed that of the extruded condition. Besides the mechanical properties, which offer stability of the implant, the corrosion rate and morphology is also of interest in biomedical applications. The corrosion rate needs to fit the healing time of the bone and the corrosion morphology needs to be as uniform as possible. Early failure because of local corrosion is not acceptable. The top views of the corroded samples after immersion are shown in Fig. 4. By visible appearance, it is already seen that the solid solution condition (Fig. 4b) corroded the most among each alloy, and WE32 (on the left) corrodes faster than WE33 (on the right). The smallest corrosion attack is seen in the precipitation-hardened condition for both alloys at 200°C after 48 h (Fig. 4d). Also, the precipitation-hardened condition at 250°C for 8 h of WE33 show only a small amount of corrosion attack.

The bar chart in Fig. 5 presents data on the corrosion rate and on the corrosion morphology, evaluated by the pitting factor. WE33 shows an overall smaller corrosion rate: 1.18 $\pm$ 0.12 mm/year for extruded, 3.91 $\pm$ 0.28 mm/year for T4, 0.18 $\pm$ 0.02 mm/year for T6-250°C-8 h and 0.44 mm/year for T6-200°C-48 h, compared to 14.60 $\pm$ 0.53 mm/ year for extruded [25].20 $\pm$ 8.1 mm/year for T4, 5.30 $\pm$ 0.43 mm/year T6-250°C-8 h for and 0.41 $\pm$ 0.05 mm/year for T6-200°C-48 h of WE32, respectively. The increase of alloying elements of $\sim$ 0.3 wt.% Y and $\sim$ 0.4 wt.% Nd and very small amounts of Gd and Dy seem to act positively. The increase in the volume fraction of the intermetallic phases, with grain boundary networks formed as well as inner grain secondary phases in the extruded condition improves the formation of a passive layer and provides a shift to a more noble alloy. From EDX spectra of the secondary phases, a stoichiometry of Mg5(Gd, Y, Dy, Nd) is suggested [24]. The solution heat-treated condition of both alloys shows the highest corrosion rate. In TEM work, which is not presented here, no precipitates could be observed. The worst corrosion rate in the solution heat-treated alloy is therefore also influenced by the growth in grain size. An influence of the different texture is also possible. Recent studies have demon-strated that the

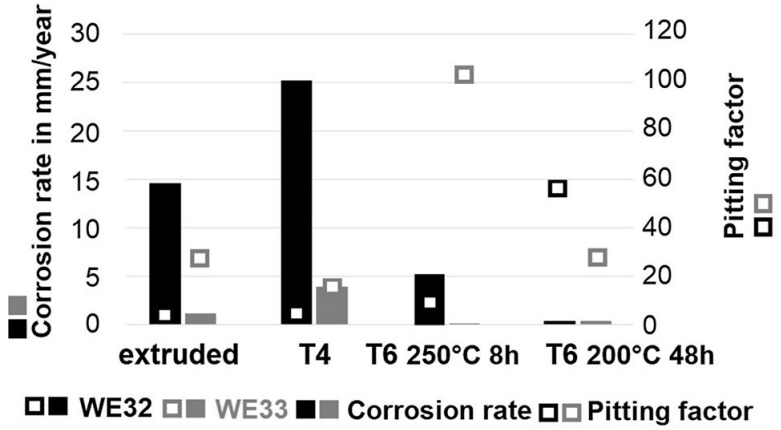

Figure 5: Corrosion rate and pitting factor of WE32 and WE33 after immersion in the conditions: extruded, T4, T6-250°C-8 h and T6-200°C-48 h, pitting factors are presented as maximum values.

corrosion performance of Mg alloys can be improved by controlling the texture [25,26]. However, here, the higher amount of alloying additions acts in a positive manner.

Micro-galvanic corrosion and precipitate strengthening is mostly influenced by the type and morphology of the precipitates, their volume fraction and spatial distribution. Especially, the precipitation-hardened conditions show reduced corrosion rate, which is very significant for the ageing treatment at 200°C for 48 h. Fine precipitates in a higher volume fraction have been already reported to give rise to lower corrosion rates [24]. They provide a sufficient amount of micro-galvanic couples between the solid solution phase and precipitates at a shorter distance, and are therefore responsible for forming a more pronounced passive layer, which eliminates the corrosion media from the surface. In contrast to these results, a study on Mg-5Y-1.5Nd by Ma [27] presented that the solid solution condition had the lowest corrosion rate and the aged conditions corroding faster, especially at shorter (6 h) and longer times (24 h), compared to the peak aged condition and corrosion pits found. Firstly all this study has been carried out in 3.5% NaCl, which is stronger than the Ringer solution (comparable with 0.9% NaCl) and the higher amount of Y causes a much higher amount of the precipitated phases, which act as micro-cathodes not leaving a passive layer to form. The positive influence Gd and Dy is investigated in the study by Ma.27 However, Ma?s27 study shows that the peak aged condition (225°C for 14 h) with the finest distribution of precipitated phases corrodes the least among the aged conditions.

In addition to the corrosion rate, the pitting factor is presented in Fig. 5 and gives important information on the corrosion morphology. A clear trend can be seen: samples with a high corrosion rate show a low pitting factor and vice versa. Corrosion pits have been found for every heat treatment condition and are mostly of a wide and shallow shape. Only a few pits are undercutting pits. Low pitting factors mean that local corrosion areas overlap and form a rough surface. A high pitting factor, especially found in the aged condition, indicates that the passive layer is not completely dense and uniform, so that corrosion pits can form and ongoing corrosion concentrates on these areas.

To describe the corrosion and its morphology in a different way, the size of the area of corrosion as a percentage as well as the depth of the nine deepest pits can be used. Using the top views from Fig. 4, it can be summarized that almost the entire surfaces of the T4 condition of WE32 (97%) and WE33 (86%) are corroded. The surface of the extruded condition of WE32 is compared to extruded WE33 corroded to significantly higher extent: 86% compared to 23%, respectively. Among the aged conditions, only the T6-250°C-8 h samples show a large amount of surface corrosion (Fig. 4c, left). As already described, the large precipitates act less positively on the corrosion rate. However, in WE33, the micro-cathodic effect between the precipitates and the α-Mg matrix seems more favorable for forming a passive layer resulting in a lower corrosion rate. The size of corroded area agrees very well with the corrosion rate. However, if very deep and large local pitting corrosion occurs (not the case here), such agreement is not necessarily seen. The 3D images in Fig. 6 are one possibility to evaluate the nine deepest pits, but the metallographic cross-sections of the corroded samples are also used and do evaluate the shape of pits in a better way (undercutting pits are not possible to evaluate by applying confocal light microscopy. However, Fig. 7 shows the nine deepest corrosion pits of the alloy WE33 which, according to Fig. 5, shows the smaller overall corrosion rate and lower pitting corrosion resistivity.

Figure 7 shows that the solid solution condition (T4) of WE33 clearly shows the deepest corrosion pits, which remain higher, up to pit number 9. Also, the extruded condition of WE33 has at least nine pits deeper than 200 μm. The heat-treated condi-tions T6-250°C-8 h of WE33 start off rather high, but only a few pits are deep. Ageing WE33 at 200°C over 48 h shows the lowest depth of corrosion pits, whereas the pits in the aged condition of WE32 at 200°C over 48 h start off rather deep; but only a few are deeper than 200 μm. That means that the pitting corrosion resistivity is rather low, and a strong local corrosion occurs after the first pits have formed.

Combining all the data for corrosion rate, deepest pits and pitting factor, the following can be stated for WE33: the extruded condition shows medium-ranged pits ($\sim$ 600 μm), has a low corrosion rate ($\sim$ 1.2 mm/year) and therefore a medium pitting factor of 26 has been found. The solid solution-treated condition (T4)

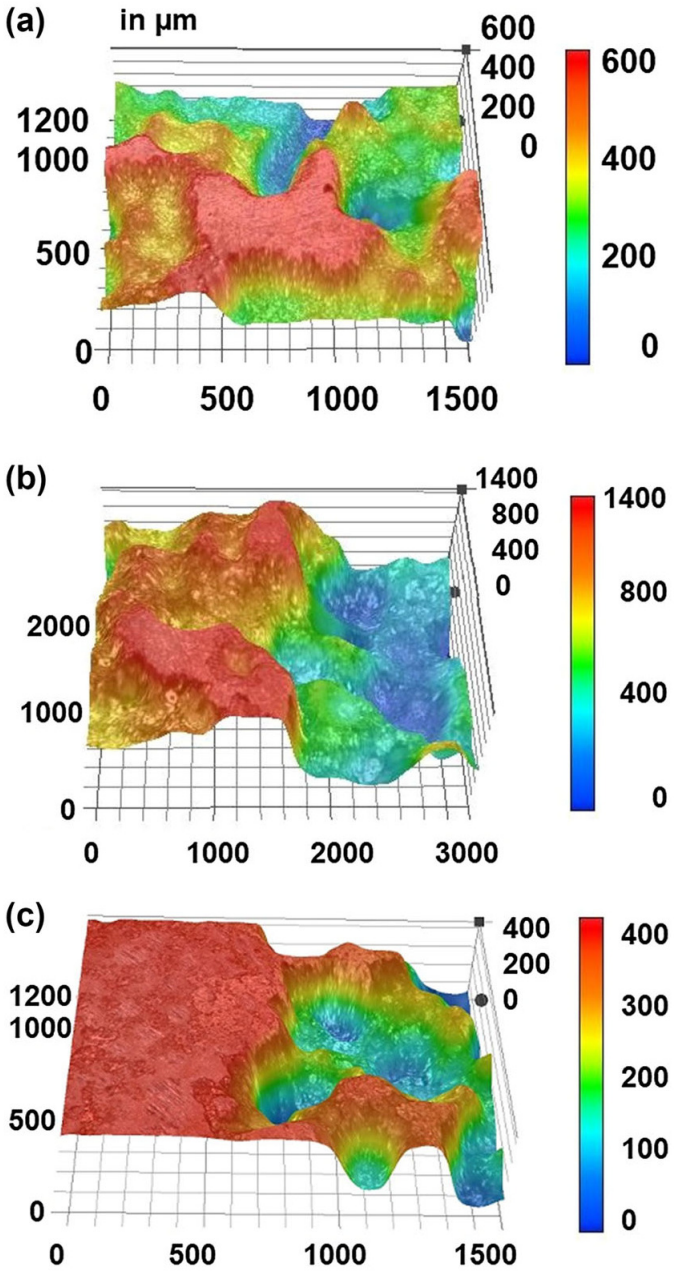

Figure 6: Corrosion morphology of WE32 by 3D imaging: (a) extruded, (b) T4 and (c) T6-250°C-8 h.

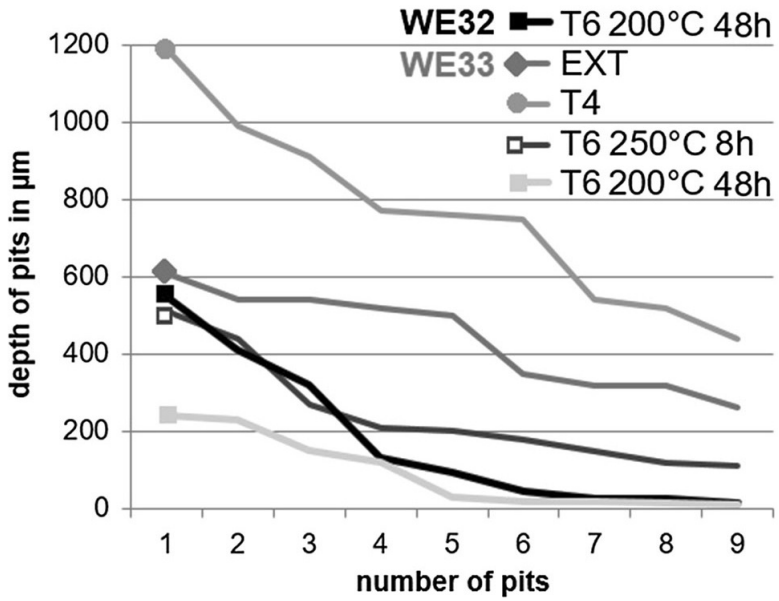

Figure 7: Nine deepest corrosion pits after immersion in WE32 in T6-200°C-48 h and WE33 in the conditions: extruded, T4, T6-250°C-8 h and T6-200°C-48 h (depth data belong to one individual sample).

shows the deepest pits (up to 1200 μm), but, since the corrosion rate is higher, a lower pitting factor of 15 is found. This is a good example that deep pits do not consequently mean high pitting factors: the ongoing corrosion forms overlapping corrosion pits, resulting in medium-ranged pits and causing a fast but uniform corrosion. Ageing WE33 at 250°C for 8 h results in one of the lowest corrosion rates, but medium-sized pits; therefore the pitting factor is the highest among all the samples investigated. Ageing WE33 at 200°C for 48 h led to the smallest pits found, the corrosion rate is also very low, and so a moderate pitting factor can be found. According to Fig. 7, WE32 at the same ageing condition shows pits in the medium range at a similar low corrosion rate, while the pitting factor is found to be higher. Thus, it appears that the higher volume fraction of fine precipitates in WE33 compared to WE32 is more beneficial to the corrosion rate in immersion in general, but also to the resistance to pitting corrosion.

Figure 8 shows the influence of heat treatment on the corrosion behavior of WE32 by representative current density-potential curves. They have been evaluated with potentiodynamic polarization. To cause a high anodic dissolution, they were run from a potential of $\sim$ 2000 mV to 500 mV. The fine-grained extruded material has a current density at around 26 mA/cm^2 at 500 mV. The solid solution-treated condition (T4) shows the highest current density values of 30 mA/cm^2 at

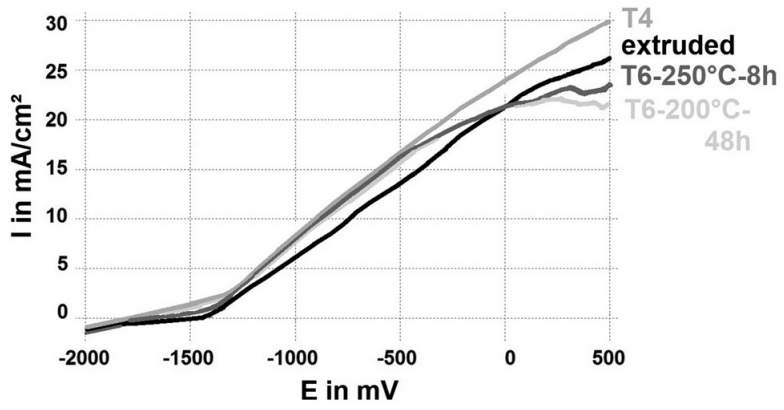

Figure 8: Influence of heat treatment on corrosion measured with potentiodynamic polarization (representative current density- potential curves) on the example of WE32 in the conditions: extruded, solution heat-treated T4 and precipitation hardened T6 at 250°C for 8 h and T6 at 200 °C for 48 h.

500 mV. Both curves show no visible breakdown potential. In WE32, the solid solution-treated condition (T4) shows a higher current density from the start, and here the coarser grain size causes higher corrosion. Due to similar grain sizes, the aged conditions corrode with a similar current density-potential curves, but at lower current density values due to the presence of precipitates. At a current density of $\sim$ 500 mV, a pseudo-passivation can be seen. The current density still increased with increas-ing potential, but at a much lower rate. The T6-200°C-48 h condition shows a decrease in current density with increasing potential from 250 mV onwards. Pseudo-passivation is usually a result of a non-uniform passive layer and a hint of pitting corrosion. The potential was kept below 500 mV as higher potentials would be unrealistic for implants within the body environment. A statement on the potential of breakdown cannot therefore be given.

The corroded area was evaluated by using the cross-sectional macrograph of the corroded end face of the cylindrical samples. The samples were ground through the cross-section of the cylinder without removing the corrosion product. Since only the inner region of the cylinder face was corroded, the initial surface (an outer ring of 1.5 mm) could be used as a reference. Sorting WE32 by the corroded amount of the corroded area (evaluated from the cross-sectional micrograph) following different treatments can be arranged in the following order: T4 (1.51 mm^2) > extruded (1.35 mm^2) > T6-250°C-8 h (1.24 mm^2) > T6-200°C-48 h (0.97 mm^2). This order agrees with the corrosion rate of the immer-sion tests and with the value of the current density at 500 mV in Fig. 8. However, not only the end value of the curves determines the corrosion rate but also the curve it-

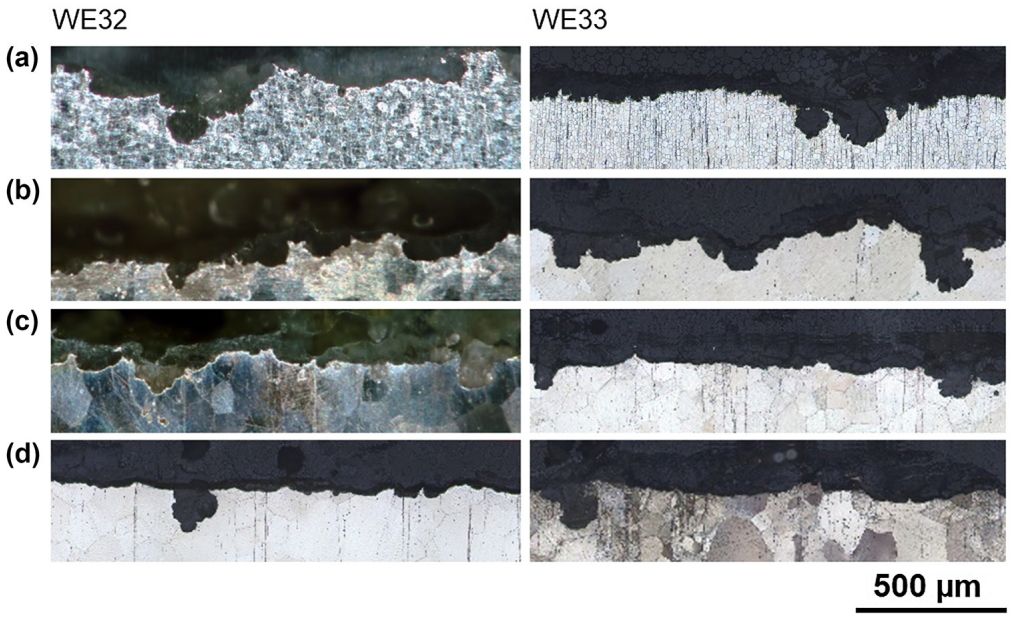

Figure 9: Cross-sectional micrographs showing corrosion morphology after polarization of WE32 and WE33: (a) extruded, (b) T4, (c) T6-250°C-8 h and (d) T6-200°C-48 h.

self. Sorting WE33 by the corroded area gives a different picture: extruded (1.60 mm^2) > T6-200°C-48 h (0.74 mm^2) > T6-250°C-8 h (0.70 mm^2) > T4 (0.67 mm^2), where the values of the heat-treated conditions are very close to each other. The extruded condition of WE33, contrary to the immersion test results, and in contrast to WE32, shows a significantly higher corrosion rate. An explanation for that cannot be given at the present. Data from the polarization and immersion measurements have been found to be different in previous research [28]. Polarization causes anodic corrosion by the increase in the applied voltage, while in immersion the material is left at its equilibrium environment. It is possible that during polarization the forming passivation layer is attacked by the increased voltage, providing a potential difference, finally causing the passivation layer to break down. The values of the corrosion rate evaluated by immersion do not show an overall agreement with the values of corroded area from polarization (since the measurement methods are different, the absolute values cannot be compared anyway). However, the values show that the corrosion rate of the T6-200°C-48 h is very low in immersion and polarization (fine precipitates act beneficially on passivation).

Figure 9(a-d) shows the representative morphologies of the corroded areas of the cross-sections for both alloys: WE32 on the left row and WE33 on the right

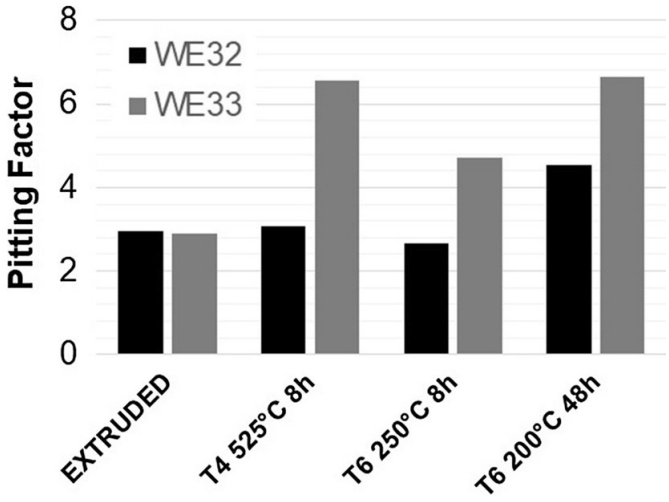

Figure 10: Pitting factor of WE32 and WE33, presented as maximum values, after polarization in the conditions: extruded, T4, T6-250°C-8 h and T6-200°C-48 h.

row. Lower magnified images of these cross-sections also include the original surface baseline, which was covered by a sealing ring during polarization and could be used to evaluate the depth of the pits. The corroded surface appears rather non-uniform, showing that roughness is indicative of corrosion pits. Pitting corrosion can be seen in each micrograph, mostly where the depth is not much larger than the width of the opening pit. A small amount of undercutting can be observed. However, these pits do not appear to be in a critical narrow and very deep shape.

Figure 10 shows the pitting factors of the alloys WE32 and WE33 and their dependence on the heat-treatment condition. Both extruded conditions show a pitting factor around 3. Ageing at T6-200°C-48 h causes the highest pitting factors: with a lower corrosion rate as a result of passivation (see Fig. 8), the pitting factor increases when the corrosion layer is obviously not dense enough, which agrees with the immersion tests. This shows that the alloy design should be carried out in a way such that the passive layer is dense and uniform. To achieve this retention, a small grain size will be beneficial.

4 Summary

This study provides a very detailed investigation of Mg-RE alloys concerning mechanical and corro-sion properties. It shows that the precipitation hardening in two Mg-Y-Nd-Gd-Dy (WE32 and WE33) alloys is an effective mechanism to

strengthen the material, as well as to modify the corrosion morphology by changing the amount and size of second phases. The mechanical properties like tensile data and hardness show that the higher the alloy element the higher the strength (values up to 170 MPa for TYS) with decreasing ductility (down to 12%). A short ageing time of 8 h is observed for peak hardness at a temperature of 250°C. Aging at 200°C leads to a longer ageing time to peak hardness and the highest hardness has been found at 48 h. The peak hardening causes hardness values exceeding the initial extruded condition, especially for the lower ageing temperature. Peak hardening reduces ductility mostly due to the large grain growth during solution heat-treatment from an average of 15-25 μm to 100-150 μm. Grain growth during ageing is not significant.

The highest corrosion rate in immersion was found in the T4 condition, to a much higher extent in WE32. Precipitation hardening shows reduced corrosion rate, especially for the ageing treatment of 200°C for 48 h. A higher volume fraction of fine precipitates provides a useful distance of micro-galvanic couples between the solid solution phase. These precipitates are therefore responsible for forming a more pronounced passive layer, which eliminates the corrosion media from the surface. On the other hand, the passive layer must be completely densified and uniform to avoid pitting corrosion. The aged condition in this study shows rather high pitting factors. However, very deep and narrow pits, which would become large stress intensifiers under mechanical loading, have not been found.

To conclude the study presented here: a fine dispersion of precipitates through optimized precipitation hardening is suggested for improved mechanical properties and corrosion rates. The higher amount of alloying additions in WE33 acts in a positive manner on the properties. However, special attention must also be paid to the homogeneous corrosion morphology. The alloys in this study do not show the best resistance to pitting corrosion. Further modification of the alloy and process design should aim to keep the grain size as small as possible.

Acknowledgements

The authors thank the Extrusion Center Berlin in Germany for extruding the bars and acknowledge the support of Hartmut Habeck and Benjamin Clausius from UAS Stralsund. Julia Bode from TU Bergakademie Freiberg, Germany, is thanked for ICP-OES measurements.

References

1. D. Zhao, F. Witte, F. Lu, J. Wang, J. Li, and L. Qin, Biomaterials 112, 287 (2016).
2. A.D. Sudholz, K. Gusieva, X.B. Chen, B.C. Muddle, M.A. Gibson, and N. Birbilis, Corros. Sci. 53, 2277 (2011).
3. M.P. Staiger, A.M. Pietak, J. Huadmai, and G. Dias, Biomaterials 27, 1728 (2006).
4. N. Hort, Y. Huang, D. Fechner, M. Stö¨rmer, C. Blawert, F. Witte, C. Vogt, H. Drücker, R. Willumeit, K.U. Kainer, and F. Feyerabend, Acta Biomater. 6, 1714 (2010).
5. H. Kalb, A. Rzany, and B. Henzel, Corros. Sci. 57, 122 (2012).
6. J.M. Seitz, A. Lucas, and M. Kirschner, JOM 68, 1177 (2016).
7. C. Rapetto and M. Leoncini, J. Thorac. Dis. 9, 903 (2017).
8. Magnesium Elektron UK, data sheet 467.
9. D. Tolnai, C.L. Mendis, A. Stark, G. Szakacs, B. Wiese, K.U. Kainer, and N. Hort, Mater. Lett. 102-103, 62 (2013).
10. B. Smola, I. Stulikova, F. von Buch, and B.L. Mordike, Mater. Sci. Eng., A 324, 113 (2002).
11. L.L. Rokhlin, T.V. Dobatkina, N.I. Nikitina, and I.E. Tarytina, Met. Sci. Heat Treat. 52, 588 (2011).
12. Y.H. Kang, D. Wu, and R.H.E. Chen, J. Magnes. Alloys 2, 109 (2014).
13. F. Feyerabend, J. Fischer, J. Holtz, F. Witte, R. Willumeit, H. Drücker, C. Vogt, and N. Hort, Acta Biomater. 6, 1834 (2010).
14. L. Yang, N. Hort, D. Laipple, D. Ho¨che, Y. Huang, K.U. Kainer, R. Willumeit, and F. Feyerabend, Acta Biomater. 9, 8475 (2013).
15. ASTM Standard G46-94, Standard Guide for Examination and Evaluation of Pitting Corrosion (Washington, DC: ASTM, 1994).
16. R.W. Revie and H.H. Uhlig, Corrosion and Corrosion Control (Hoboken: Wiley, 2008), p. 17.
17. Z. Ahmad, Principles of Corrosion Engineering and Corrosion Control (Oxford: Butterworth-Heinemann, 2006), p. 266.
18. F. Witte, J. Fischer, J. Nellesen, C. Vogt, J. Vogt, T. Donath, and F. Beckmann, Acta Biomater. 6, 1792 (2010).

19. V. Kree, J. Bohlen, D. Letzig, and K.U. Kainer, Pract. Metallogr. 41, 233 (2004).

20. N. Li, C. Guo, Y.H. Wu, Y.F. Zheng, and L.Q. Ruan, Corros. Eng., Sci. Technol. 47, 346 (2012).

21. P. Maier, S. Gavras, M. Freese, G. Schott, and N. Hort, in Proceedings of the 11th International Conference on Magnesium Alloys and their Applications: Mg2018, Old Windsor, UK (2018).

22. Y. Zheng, Magnesium Alloys as Degradable Biomaterials (Boca Raton: CRC Press, 2015), p. 345.

23. S. Gorsse, C.R. Hutchinson, B. Chevalier, and J.F. Nie, J. Alloys Compd. 392, 253 (2005).

24. P. Maier, R. Peters, C.L. Mendis, S. Mu¨ller, and N. Hort, JOM 68, 1183 (2016).

25. D. Orlov, K.D. Ralston, N. Birbilis, and Y. Esttin, Acta Mater. 59, 6176 (2011).

26. L.G. Bland, B.C. Rincon Troconis, R.J. Santucci, J.M. Fitz-Gerald, and J.R. Scully, Corrosion 72, 1226 (2016).

27. X. Ma, Q. Jiang, Y. Li, and B.R. Hou, Int. J. Electrochem. (2016).

28. P. Maier, M. Bechly, and N. Hort, in Contributed Papers from Materials Science and Technology?MS&T17, p. 76 (2017).